Membrane-protein binding measured with solution-phase plasmonic nanocube sensors

Hung-Jen Wu[1–3], Joel Henzie[2], Wan-Chen Lin[1,2], Christopher Rhodes[1,2,4], Zhu Li[5], Elodie Sartorel[5], Jeremy Thorner[5], Peidong Yang[2] & Jay T Groves[1–3,6]

We describe a solution-phase sensor of lipid-protein binding based on localized surface plasmon resonance (LSPR) of silver nanocubes. When silica-coated nanocubes are mixed in a suspension of lipid vesicles, supported membranes spontaneously assemble on their surfaces. Using a standard laboratory spectrophotometer, we calibrated the LSPR peak shift due to protein binding to the membrane surface and then characterized the lipid-binding specificity of a pleckstrin homology domain protein.

The intracellular environment is dominated by membrane surfaces, and a significant fraction of biochemical processes involves membranes[1]. Analytical methods for membrane analysis based on chemical labeling have many drawbacks, and hence there is substantial demand for quantitative label-free detection. Techniques to study lipid-protein interactions such as backscattering interferometry[2], colloidal assembly[3], nanowire arrays[4], microcantilevers[5], acoustic sensing[6] and surface plasmon resonance (SPR)[7] have all been reported, but most are impractical for widespread adoption. A more promising method is LSPR, in which protein binding to a membrane substrate causes measurable changes in refractive index near sensor surfaces[8–11]. However, conventional LSPR techniques typically rely on analyte capture on nanofabricated surfaces and often require sophisticated instrumentation. The need for quantitative label-free detection methods that are simple, robust and accessible to scientists using generic laboratory equipment remains unmet.

Here we report a platform that enables label-free measurements of protein binding to membrane surfaces on a standard laboratory spectrophotometer. We previously described label-free detection using LSPR of thiolated silver nanocubes immobilized on flat substrates[9]. This configuration required multiple reactions and a customized detection system, ultimately proving to be as impractical as other methods. By modifying the system to allow measurement entirely in the solution phase, we have substantially improved its utility. Highly monodisperse silver (Ag) nanocubes were prepared by an established synthetic protocol[12] (**Supplementary Fig. 1**). To create a favorable surface for membrane assembly and suspension in solution, an ultrathin layer of silica was then grown using Stöber synthesis (Online Methods). Transmission electron microscopy (TEM) micrographs revealed a uniform silica shell covering the Ag surface with an average thickness of 3.9 ± 0.2 nm ($n = 5$, mean ± s.d.) and corners with a curvature radius of 19 nm (**Fig. 1a**,**b**). Elemental maps acquired by high-angle annular dark-field scanning TEM showed that the silicon and oxygen intensities were strongest at the edges of Ag@SiO_2 core-shell nanocube particles (silver core @ silica shell), indicating that the shell is conformal and uniform (**Fig. 1c–f** and **Supplementary Fig. 2**). Additionally, the SiO_2 coating provides a shelf life in excess of 1 year by slowing silver oxidation.

Ag@SiO_2 nanocubes exhibit a sharp quadrupolar LSPR scattering peak (**Fig. 1g**). This is easily observed in the extinction spectrum of a suspension of nanocubes using standard laboratory tools such as a transmission ultraviolet-visible spectrophotometer, a microvolume spectrometer (for example, NanoDrop), a dark-field microscope (**Supplementary Fig. 3**) or a light-scattering spectrophotometer (**Supplementary Fig. 4**). Electromagnetic simulations based on the actual particle geometry confirm that the time-averaged electric field norms ($|E|/E_0$) exhibit quadrupole resonance with the highest near-field enhancement near the nanocube corners (**Fig. 1h**). At quadrupole resonance, $|E|/E_0$ decays to 50% of its value at the silica-medium interface over a distance of about 10 nm. The silica layer is sufficiently thin that the LSPR field still penetrates a lipid bilayer of 3–5 nm thickness (**Supplementary Fig. 5**). A widely used figure of merit (FOM) for LSPR is the peak shift (in nm) per refractive index unit normalized to the line width of the LSPR peak (Online Methods). The FOM for Ag@SiO_2 nanocubes is 1.7, as compared to 2.4 for bare silver nanocubes.

Supported lipid bilayers form spontaneously upon mixing Ag@SiO_2 nanocubes in a lipid-vesicle suspension (**Fig. 1g**). Fluorescence recovery after photobleaching confirmed the lateral fluidity and connectivity of membranes covering substrate-adsorbed nanocubes[9]. A supported bilayer formed on top of both the nanocubes and the glass substrate and exhibited recovery behavior almost identical to that of membranes on bare glass substrates, thus indicating that membranes on the nanocubes were

[1]Howard Hughes Medical Institute, University of California, Berkeley, California, USA. [2]Department of Chemistry, University of California, Berkeley, California, USA. [3]Physical Biosciences Division, Lawrence Berkeley National Laboratory, Berkeley, California, USA. [4]Department of Mechanical Engineering, University of California, Berkeley, California, USA. [5]Department of Molecular and Cell Biology, Division of Biochemistry, Biophysics and Molecular Biology, University of California, Berkeley, California, USA. [6]Materials Sciences Division, Lawrence Berkeley National Laboratory, Berkeley, California, USA. Correspondence should be addressed to J.T.G. (jtgroves@lbl.gov).

RECEIVED 15 JUNE; ACCEPTED 11 SEPTEMBER; PUBLISHED ONLINE 21 OCTOBER 2012; DOI:10.1038/NMETH.2211

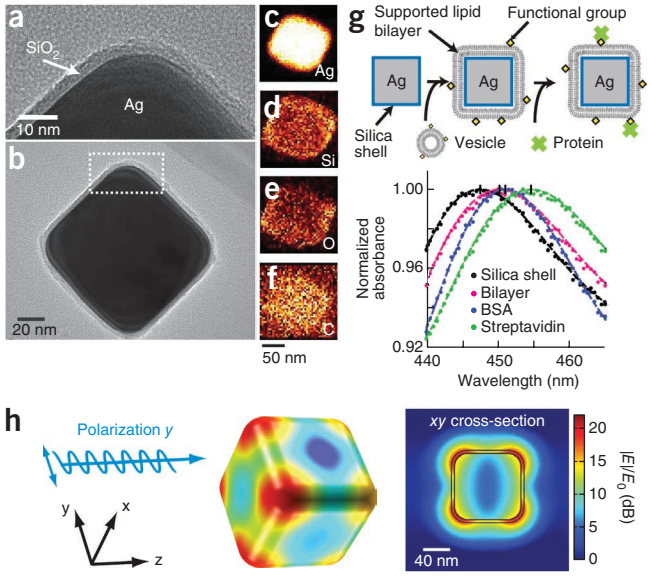

Figure 1 | Physical properties of $Ag@SiO_2$ core-shell nanocubes. (**a**,**b**) TEM images of a $Ag@SiO_2$ nanocube. (**a**) Magnified image of region denoted by dotted box in **b**. (**c**–**f**) Elemental maps obtained by high-angle annular dark-field scanning TEM with energy-dispersive X-ray spectroscopy. The elements are silver (**c**), silicon (**d**), oxygen (**e**) and carbon (**f**). (**g**) Top, detection procedure of nanocube sensors. Supported lipid bilayers are formed by vesicle fusion onto the silica surface, and protein binding is monitored by shifts in the LSPR extinction spectrum. Bottom, typical spectra of membrane coverage and protein binding to the membrane surfaces. Sequential addition of lipid vesicles, BSA and streptavidin causes LSPR red shifts. (**h**) Electric field norm ($|E|/E_0$) in decibels of a nanocube at resonance (n = 1.33303, λ_0 = 474 nm) computed using finite-element analysis.

connected and fluid (**Supplementary Fig. 6**). The magnitude of fluorescence recovery indicates that the majority of nanocubes were covered with lipid membrane. In contrast, uncoated Ag nanocubes on a glass substrate exhibited similar recovery times but only 60% of the fluorescence magnitude of glass alone, illustrating that lipids adsorbed on bare nanocubes do not form a fluid and continuous bilayer with the surrounding fluid bilayer. Although it has been suggested that a supported lipid bilayer cannot form on a highly curved surfaces (defined by a ≤11-nm radius of curvature) because of high elastic energy[13], we did not observe any such limitation on the $Ag@SiO_2$ nanocubes (which have a 19-nm radius of curvature at the corner).

We calibrated the LSPR response of the system by monitoring the essentially irreversible binding of streptavidin to biotinylated lipids in the nanocube supported membrane (**Supplementary Fig. 7**). We used three different approaches to control the surface density of membrane-bound streptavidin: (i) titrating biotinyl-cap–PE in bilayer, (ii) titrating streptavidin in solution and (iii) measuring unbound fluorescent streptavidin (**Supplementary Discussion**).

LSPR shifts were measured at different known surface densities of streptavidin and exhibited a linear relation with protein density (**Fig. 2a**). Consistent LSPR responses of 0.191 ± 0.025 ng mm^{-2} nm^{-1} (n = 3, mean ± s.d.) were determined by three independent approaches (**Supplementary Table 1**).

To assess whether bilayer-coated $Ag@SiO_2$ nanocubes can quantify protein binding accurately, we compared the system with the established method of multicomponent fluorescence correlation spectroscopy (FCS)[14] using cholera toxin subunit B (CTB) binding to the membrane-associated receptor G_{M1} as a model system (**Fig. 2b**). Lipid vesicles and CTB were labeled with different fluorophores, and the concentrations of bound and unbound CTB were monitored by multicomponent FCS measurements. The average vesicle size was determined independently by dynamic light scattering, thereby allowing the surface density of vesicle-bound CTB to be calculated (details in **Supplementary Discussion**). Using the same materials and experimental conditions, nanocube measurements were performed independently. LSPR response was converted to protein surface density using the LSPR response to protein mass change measured in the biotin-streptavidin system, 0.191 ng mm^{-2} nm^{-1} (**Supplementary Table 1**). Both multicomponent FCS and nanocube methods reached equilibrium state and the same surface density after 1,000 s (**Fig. 2b**). The similar correlations between LSPR shift and protein mass density measured in the biotin-streptavidin and CTB-G_{M1} systems with four independent approaches demonstrated the ability of the nanocube sensors to quantify

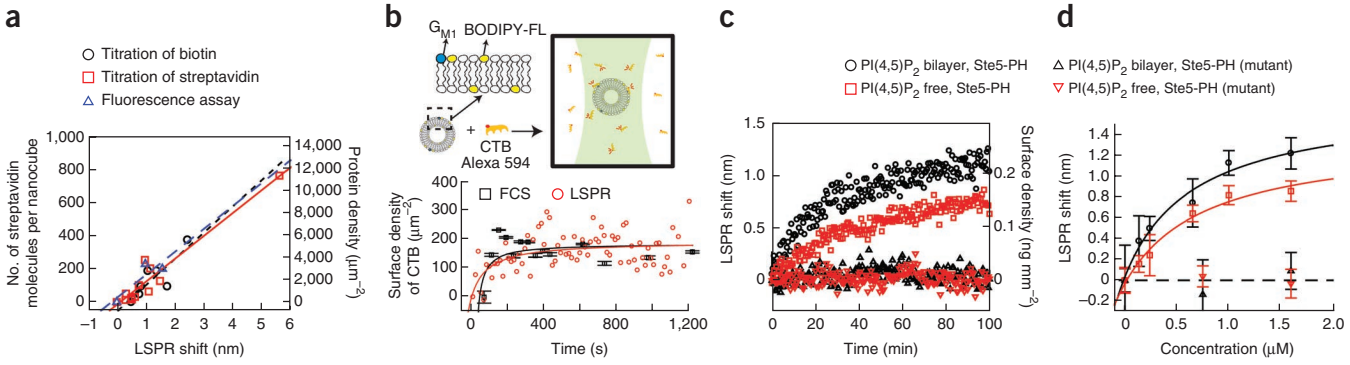

Figure 2 | Calibration of the nanocube assay. (**a**) Relation between LSPR shift and number of streptavidin molecules per nanocube (left vertical axis) and surface density (right axis) measured by titration of biotinyl-cap–PE, titration of streptavidin and fluorescence measurement of streptavidin concentration. Linear fit slopes are reported in **Supplementary Table 1**. (**b**) Top, concentrations of bound and unbound cholera toxin subunit B (CTB) are detected by multicomponent fluorescence correlation spectroscopy (FCS). Alexa Fluor 594–CTB binds to vesicles (average diameter, 120 nm) containing 0.5% G_{M1} and 0.5% BODIPY-FL-DHPE lipids. BODIPY-FL-DHPE was used to determine the average number of vesicles diffusing within the excitation spot. Bottom, binding kinetics measured by multicomponent FCS and nanocube assay. (Error bars of FCS, n = 20, mean ± s.d.) (**c**) Binding kinetics of wild type and R407S K411S mutant of Gst-Ste5 PH to different membrane surfaces. Concentrations: Gst-Ste5 PH, 1.6 μM; Gst-Ste5 PH mutant, 1.6 μM. (**d**) Equilibrium binding curves of Gst-Ste5 PH to bilayers (n = 3, mean ± s.e.m.).

protein binding (**Supplementary Table 1**). It is worth noting that unlike FCS, which works only at low concentration, the nanocube detection strategy has a much broader working range (**Supplementary Discussion**). The additional labeling required by FCS also limits its applications.

Finally, we used the Ag@SiO_2 nanocube assay to determine the previously unknown lipid binding specificity of Ste5, a prototypical mitogen-activated protein kinase (MAPK) scaffold protein that delivers its kinase cargo to the plasma membrane to initiate downstream signaling. Ste5 contains a pleckstrin homology (PH) domain (residues 388–518) that is required for its membrane recruitment and function, but the dependence of Ste5 binding on membrane composition is not well known[15]. We investigated the binding of Ste5 to membranes with and without $PI(4,5)P_2$. Gst-Ste5 PH-domain fusion proteins (corresponding to Ste5 residues 369–517), with and without R407S and K411S mutations thought to abrogate lipid binding, were constructed, expressed and purified from *Escherichia coli*. To avoid interference of detergent with the membrane assay, we eliminated its use during protein purification (**Supplementary Discussion**). Only wild-type Gst-Ste5 PH domain bound to the membrane surface (**Fig. 2c**). Although more Ste5 binding was observed on $PI(4,5)P_2$ membranes, appreciable binding was also observed on membranes without $PI(4,5)P_2$. This may be due to the presence of phosphatidic acid lipids, which have been observed to associate with PH domains in other protein systems[16]. Binding curves were established to compute the binding affinity of Gst-Ste5 on different compositions of membranes (**Fig. 2d**, $K_d = 0.49 \pm 0.33$ μM ($PI(4,5)P_2$ bilayer) and 1.6 ± 0.45 μM ($PI(4,5)P_2$-free bilayer)). At similar lipid compositions, we have previously reported rough estimates of K_d for Ste5-membrane binding using filter-immobilized lipids, liposome flotation assays and SPR that suggest a dissociation constant in the range of 5–10 μM (ref. 15). However, the lipid immobilization and tethering required for the filter and SPR assays are disruptive of the membrane surface environment[7], and liposome flotation assays are intrinsically error prone. Thus, among all of the measurements, the nanocube assay is the most consistent, and we argue that it is most accurate.

We report a core-shell Ag@SiO_2 nanocube sensor that can measure protein binding to its membrane-coated surfaces. No complicated fabrication is necessary, and the sensors can be prepared on the gram scale (>10^{14} nanocubes) at minimal cost. Solution-phase measurements readily integrate 10^{12} nanocubes in the illumination area of a standard spectrophotometer cuvette. This provides a high sensitivity of approximately 0.19 ng cm^{-2} based on 0.01-nm standard error of 20 consecutive LSPR measurements (**Supplementary Discussion**), in contrast to the immobilized format[9] (10^9 nanocubes; sensitivity = 1.5 ng cm^{-2}). Solution LSPR is applicable to analytes that bind lipid membranes or membrane proteins, including proteins, peptides, nucleic acids or even entire cells. Simply adding Ag@SiO_2 nanocubes to a vesicle suspension produces a system in which analyte binding to the membrane surface can be read out by standard spectral technique available in most laboratories, without the need for labeling.

METHODS

Methods and any associated references are available in the online version of the paper.

Note: Supplementary information is available in the online version of the paper.

ACKNOWLEDGMENTS

This work was supported by the Director, Office of Science, Office of Basic Energy Sciences, of the US Department of Energy under contract no. DE-AC02-05CH11231 (to J.T.G.) and by US National Institutes of Health Research Grant GM21841 (to J.T.). P.Y. would like to acknowledge the support from King Abdulaziz University.

AUTHOR CONTRIBUTIONS

H.-J.W. and J.T.G. conceived the solution-phase nanocube sensor strategy. H.-J.W. implemented the experiments, J.H. synthesized nanocubes and performed TEM, W.-C.L. performed FCS measurements, C.R. performed LSPR simulations and Z.L. and E.S. prepared Ste5 proteins. H.-J.W., C.R. and J.T.G. wrote the manuscript. J.T.G., J.T. and P.Y. supervised the project. All authors discussed the results and commented on the manuscript at all stages.

COMPETING FINANCIAL INTERESTS

The authors declare no competing financial interests.

Published online at http://www.nature.com/doifinder/10.1038/nmeth.2211. Reprints and permissions information is available online at http://www.nature.com/reprints/index.html.

1. Groves, J.T. & Kuriyan, J. *Nat. Struct. Mol. Biol.* **17**, 659–665 (2010).
2. Baksh, M.M., Kussrow, A.K., Mileni, M., Finn, M.G. & Bornhop, D.J. *Nat. Biotechnol.* **29**, 357–360 (2011).
3. Baksh, M.M., Jaros, M. & Groves, J.T. *Nature* **427**, 139–141 (2004).
4. Zheng, G., Patolsky, F., Cui, Y., Wang, W.U. & Lieber, C.M. *Nat. Biotechnol.* **23**, 1294–1301 (2005).
5. Braun, T. *et al. Nat. Nanotechnol.* **4**, 179–185 (2009).
6. Cooper, M.A. *J. Mol. Recognit.* **17**, 286–315 (2004).
7. Beseničar, M., Maček, P., Lakey, J.H. & Anderluh, G. *Chem. Phys. Lipids* **141**, 169–178 (2006).
8. Dahlin, A. *et al. J. Am. Chem. Soc.* **127**, 5043–5048 (2005).
9. Galush, W.J. *et al. Nano Lett.* **9**, 2077–2082 (2009).
10. Jonsson, M.P., Jonsson, P., Dahlin, A.B. & Hook, F. *Nano Lett.* **7**, 3462–3468 (2007).
11. Baciu, C.L., Becker, J., Janshoff, A. & Sonnichsen, C. *Nano Lett.* **8**, 1724–1728 (2008).
12. Tao, A., Sinsermsuksakul, P. & Yang, P. *Angew. Chem. Int. Ed.* **45**, 4597–4601 (2006).
13. Roiter, Y. *et al. Langmuir* **25**, 6287–6299 (2009).
14. Middleton, E.R. & Rhoades, E. *Biophys. J.* **99**, 2279–2288 (2010).
15. Garrenton, L.S., Young, S.L. & Thorner, J. *Genes Dev.* **20**, 1946–1958 (2006).
16. Zhao, C., Du, G.W., Skowronek, K., Frohman, M.A. & Bar-Sagi, D. *Nat. Cell Biol.* **9**, 706–712 (2007).

ONLINE METHODS

Materials. Lipids. The following lipids were purchased from Avanti Polar Lipids: 1,2-dioleoyl-*sn*-glycero-3-phosphocholine (DOPC); 1,2-dioleoyl-*sn*-glycero-3-phosphoethanolamine-*N*-(cap-biotinyl) (biotinyl-cap–PE); ganglioside G_{M1} (G_{M1}); 1,2-dioleoyl-*sn*-glycero-3-phospho-L-serine (DOPS); 1,2-dioleoyl-*sn*-glycero-3-phosphate (DOPA); 1,2-dioleoyl-*sn*-glycero-3-phosphoethanolamine (DOPE); L-α-phosphatidylinositol (PI); and L-α-phosphatidylinositol-4,5-bisphosphate ($PI(4,5)P_2$). The fluorescent lipid probes, Texas red 1,2-dipalmitoyl-*sn*-glycero-3-phosphoethanolamine (Texas red DPPE) and *N*-(4,4-difluoro-5,7-dimethyl-4-bora-3a,4a-diaza-*s*-indacene-3-propionyl)-1,2-dihexadecanoyl-*sn*-glycero-3-phosphoethanolamine, triethylammonium salt (BODIPY-FL-DHPE), were purchased from Invitrogen.

Ethanol (200 proof), tetraethyl orthosilicate (TEOS), 28% ammonium hydroxide solution, unlabeled recombinant streptavidin and bovine serum albumin were purchased from Sigma-Aldrich. The fluorescent proteins Alexa Fluor 647–streptavidin and cholera toxin subunit B (CTB)–Alexa Fluor 594 were purchased from Invitrogen. Streptavidin and CTB binding experiments were performed in 1× PBS buffer (Mediatech). Gst-Ste5 binding measurements were performed in HKME buffer (20 mM HEPES-KOH at pH = 7.0, 160 mM KOAc, 1 mM $MgCl_2$ and 0.1 mM EGTA).

Silica-coated nanocube. Ag nanocubes were synthesized using the polyol method[12,17,18], capped with poly(vinylpyrrolidone) (PVP) and stored in ethylene glycol before use. Ag nanocubes were coated with silica shells using the Stöber process[19]. The concentration of ammonium hydroxide and reaction time affected the thickness and quality of the silica layer[20]. The Ag nanocubes were first washed extensively with ethanol. Silica layers were coated by mixing 7.5 ml of Ag nanocube suspension in ethanol with 1,950 µl of water, 600 µl of TEOS and 300 µl of 0.28% ammonium hydroxide. The solution was sonicated during the entire reaction. After a 40-min reaction, the resulting $Ag@SiO_2$ nanocubes were washed with ethanol to remove the reagents and then washed extensively with water. The $Ag@SiO_2$ nanocubes were stored in deionized water for future use.

LSPR measurement. Various approaches have been reported to collect nanoparticle extinction spectra[21]. We used a general transmission ultraviolet-visible (UV-vis) spectrophotometer (Cary 100, Varian). Typically, spectral shifts were monitored by detecting the prominent quadrupolar LSPR peak λ_{max}. These peaks were determined by fitting transmission spectra to a seventh-order polynomial (**Fig. 1g**). The dependence of LSPR peak shift on refractive index was measured in water-glycerol solutions of various ratios. To explore the effect of the silica shell, the refractive index sensitivity of $Ag@SiO_2$ nanocubes was compared to that of Ag nanocubes using solutions of water and glycerol. (**Supplementary Fig. 8**). LSPR sensitivity was quantified using the widely reported figure of merit (FOM) calculated by dividing refractive index sensitivity by the line width of the resonance spectrum ($FOM = S/\Delta\lambda$)[22,23]. The refractive index sensitivity (S) was evaluated from **Supplementary Figure 8** and represented as peak shift (reported in nm or eV) per refractive index unit (RIU). The line width of the resonance spectrum ($\Delta\lambda$) was obtained from the full width at half-maximum of the LSPR peak (**Fig. 1g**).

To demonstrate the applicability of other detection schemes, scattering spectra were also measured by (i) dark-field scattering microscopy using a dark-field condenser and spectrometer (USB2000, Ocean Optics) and (ii) a fluorescence spectrophotometer (Varian) configured for 90° scattering detection.

The nanocube concentrations were determined by counting deposited nanocubes on glass substrates. The silica-coated nanocube solutions were incubated in a sedimentation chamber for 2 days to create monolayers of nanocubes. Dark-field microscopy was used to observe the nanocubes deposited on the bottom of each sedimentation chamber. A homemade image-analysis program was developed to count the number of nanocubes in each imaging frame.

Bilayer preparation. Lipid vesicles were prepared as follows. The desired composition of lipids was first mixed in chloroform. The mixture was then dried in a round-bottom flask and desiccated under nitrogen for at least 30 min. Lipid films were then hydrated with 18.2 M cm deionized (DI) water. The resulting suspension was probe sonicated to clarity in an ice bath and ultracentrifuged at 4 °C for 45 min. The top small-unilamellar-vesicle (SUV) solution was extracted for use in experiments. For FCS and GSst-Ste5 binding experiments, SUVs were prepared through an extrusion process. Instead of undergoing sonication, the hydrated lipids were extruded through 100 nm polycarbonate pore filters (Whatman) until the suspension reached clarity. The vesicle used in FCS measurement contained 0.5% G_{M1}, 0.5% BODIPY-FL-DHPE and 99% DOPC lipids. The lipid membranes used in Gst-Ste5 PH binding experiment contained (i) 53% DOPC, 22% DOPE, 10% DOPS, 5% DOPA and 10% PI for the PIP_2-free bilayer and (ii) 53% DOPC, 22% DOPE, 10% DOPS, 5% DOPA, 5% PI and 5% $PI(4,5)P_2$ for the PIP_2 bilayer.

Supported lipid bilayers were formed by adapting a standard vesicle-fusion technique[3]. Bilayers were assembled by combining equal volumes of SUV suspension and the desired buffer in a small centrifuge tube and vortex mixing. Excess vesicles and salt were removed by rinsing twice with the buffer using a benchtop centrifuge (minicentrifuge, VWR, maximum RCF = 2,000*g*). Membrane-coated particles were then diluted to the desired working concentration and introduced into the spectrophotometer cell.

Protein binding measurement. Bilayer-coated nanocubes were incubated with 0.05 mg ml^{-1} BSA solution to block nonspecific binding before adding desired proteins. Fifteen consecutive scans were performed to obtain the average λ_{max} of the LSPR quadrupolar peak as a baseline. The desired amount of protein was directly cast into the spectrophotometer cell (400 µl sample volume), and then pulse vortexing was performed on the mixture. Spectra in the range of 430–480 nm were scanned immediately after mixing at 0.5-nm spectral resolution. The maximum attainable scanning rate was 6 s per spectrum, limited by the configuration of the UV-vis spectrophotometer. To minimize the use of protein in Gst-Ste5 binding experiments, these measurements were performed with a sub-microvolume optical cuvette. Different volumes of protein (0.5–15 µl) were incubated with 20 µl of bilayer-coated $Ag@SiO_2$ nanocube sensors for 2 h. The average λ_{max} values of the LSPR quadrupolar peak were obtained from ten consecutive spectra. All experiments were performed at room temperature.

doi:10.1038/nmeth.2211

Fluorescence correlation spectroscopy. Fluorescence correlation spectroscopy (FCS) measurements were performed on a home-built FCS apparatus based on a Nikon TE2000 inverted fluorescence microscope as described previously[24]. Two laser beams, 488 nm and 568 nm, were coupled into an optical fiber and focused by a 100× TIRF objective (Nikon) onto the sample to excite the fluorescent probes. The emitted light was filtered through notch filters and a confocal pinhole then separated by a 560-nm long-pass filter. Before focusing onto two avalanche photodiodes (APDs) (Perkin Elmer), two color filters were used to minimize spectrum cross-talk. The photon arrival time was recorded and the autocorrelation functions of the two APD signals were calculated with a hardware correlator (Correlator.com) in real time. Using a double-labeled supported lipid bilayer as a sample, overlapping detection volumes were obtained by careful alignment of a collimator lens after the optical fiber and fine adjustment of the objective lens correction collar[25]. Measurements were made in eight-well chambered coverglasses (Nunc) that were first soaked with 0.1 M NaOH for 20 min to clean the bottom surface. The supported lipid bilayers (100% DOPC) were formed on the bottom surface by vesicle fusion. The chamber was incubated with 0.1 mg ml^{-1} BSA to prevent protein and vesicle absorption. The size and the structure factor *s* of the excitation volume were calibrated using 200 nM fluorescein in 1M NaOH solution with a known diffusion coefficient ($D = 300\ \mu m^2\ s^{-1}$)[26]. All other measurements were performed at 24.5 °C in 1× PBS buffer.

The model system, CTB binding to vesicles containing the membrane-associated receptor monosialoganglioside G_{M1}, was selected to directly compare FCS and nanocube measurements. To obtain a narrow size distribution of vesicles, SUVs were prepared by the standard extrusion method described above. Vesicles of 120-nm average diameter containing 0.5% G_{M1}, 0.5% BODIPY-FL-DHPE and 99% DOPC lipids were measured by dynamic light scattering (Brookhaven Instruments). A detailed description of the multicomponent FCS calculations is in the **Supplementary Discussion**.

Transmission electron microscopy. $Ag@SiO_2$ nanocubes were imaged using high-resolution transmission electron microscopy (JEOL 2100-F, 200 kV). The elemental X-ray analysis maps were generated using high-angle annular dark-field scanning TEM (HAADF-STEM) with an energy-dispersive X-ray spectroscopy (EDS) detector. TEM images revealed for nanocubes a lateral dimension of 98 nm, radius of curvature at the edges of 19 nm and silica-shell thickness of 3.9 nm.

LSPR simulation. Finite-element simulations using COMSOL were used to model the LSPR of silica-coated silver nanocubes. Free tetrahedral meshing of the geometry observed in TEM was performed in COMSOL and further refined in the vicinity of the silica shell. The final mesh contained 359,000 tetrahedral elements, and convergence of absorption spectra within 0.1% error was confirmed by comparing results from a coarser mesh.

Frequency-domain scattered electric field solutions were computed using COMSOL's RF module for a background oscillating field of arbitrary amplitude 1 V m^{-1}. Real and imaginary refractive index dispersion was interpolated from literature tables for silver and silica[27]. The nanocube was simulated inside a sphere of diameter 400 nm, sufficiently large for all near-field effects to be negligible at the system boundary. A perfectly matched layer (PML) was additionally incorporated to cancel any reflection artifacts in the simulation. Field solutions were calculated for 50–100 different frequencies at a time.

Gst-Ste5 Protein preparation. Gst-Ste5 PH domain fusion proteins with and without R407S K411S mutations (corresponding to Ste5 residues 369–517) were constructed, expressed and purified from *Escherichia coli* as described by Garrenton *et al.*[15]. The use of Tween-20 detergent was omitted during protein purification to avoid the influence of detergent on lipid bilayers. Prior to binding experiments, Gst-Ste5 proteins were treated with Amicon centrifuge filters (Millipore) for further purification and buffer exchange.

17. Fievet, F., Lagier, J.P., Blin, B., Beaudoin, B. & Figlarz, M. *Solid State Ionics* **32–33** (Part 1), 198–205 (1989).
18. Sun, Y. & Xia, Y. *Science* **298**, 2176–2179 (2002).
19. Stöber, W., Fink, A. & Bohn, E. *J. Colloid Interface Sci.* **26**, 62–69 (1968).
20. Sioss, J.A., Stoermer, R.L., Sha, M.Y. & Keating, C.D. *Langmuir* **23**, 11334–11341 (2007).
21. Willets, K.A. & Van Duyne, R.P. *Annu. Rev. Phys. Chem.* **58**, 267–297 (2007).
22. Sherry, L.J. *et al. Nano Lett.* **5**, 2034–2038 (2005).
23. Mayer, K.M. & Hafner, J.H. *Chem. Rev.* **111**, 3828–3857 (2011).
24. Forstner, M.B., Yee, C.K., Parikh, A.N. & Groves, J.T. *J. Am. Chem. Soc.* **128**, 15221–15227 (2006).
25. Bacia, K. & Schwille, P. *Nat. Protoc.* **2**, 2842–2856 (2007).
26. Chen, Y., Müller, J.D., Eid, J.S. & Gratton, E. in *New Trends in Fluorescence Spectroscopy: Applications to Chemical and Life Sciences* (eds. Valeur, B. & Brochon, J.-C.), Ch. 14–15, 277–302 (Springer, Berlin, 2001).
27. Palik, E.D. *Handbook of Optical Constants of Solids* (Academic, Amsterdam, 1998).